Strong magnon-magnon coupling between ferromagnetic resonances in $Co_{90}Zr_{10}/Ta/Fe_{20}Ni_{80}$ multilayers

Keke Ma,[1] Chaozhong Li,[1] Zhenhui Hao,[1] C. K. Ong,[1,2] and Guozhi Chai[1,*]

[1]*Key Laboratory for Magnetism and Magnetic Materials of the Ministry of Education, Lanzhou University, Lanzhou, 730000, People's Republic of China*

[2]*Department of Physics, Xiamen University Malaysia, Jalan Sunsuria, Bandar Sunsuria, 43900, Sepang, Selangor, Malaysia*

(Received 22 April 2023; revised 29 August 2023; accepted 1 September 2023; published 13 September 2023)

We investigate the magnon-magnon coupling between the ferromagnetic resonances (FMRs) from different ferromagnetic layers in $Co_{90}Zr_{10}$(100 nm)/Ta/$Fe_{20}Ni_{80}$(100 nm) multilayers by using broadband ferromagnetic resonance. The strong coupling between two FMRs through interlayer exchange interaction is realized due to the fact that the thicknesses of both the ferromagnetic layers far exceed the corresponding exchange length. Moreover, we find that the coupling strength can be tuned by changing the thickness of the nonmagnetic Ta layer, revealing inversely proportional relationship between the coupling strength and the thickness of the nonmagnetic Ta layer. The coupling field and coupling efficiency can be regulated by varying the anisotropy of the ferromagnetic layers via oblique deposition. Furthermore, the coupling between FMR and perpendicular standing spin waves can also be achieved with suitable anisotropy and external magnetic field. These observations demonstrate that the ground state magnonic system provides a simple ideal platform for strong magnon-magnon coupling.

DOI: 10.1103/PhysRevB.108.094422

I. INTRODUCTION

Hybrid quantum systems based on collective spin excitation in ferromagnetic (FM) materials, called magnons, have been widely studied in the past few decades, which provides a promising platform for applications of magnon-based functional devices and the development of new quantum information technology [1–3], such as quantum computing [4,5], quantum communication [6,7], and quantum sensing [8,9]. Magnons are highly adjustable quasiparticles, and can easily be designed to couple with a variety of dynamic media and platforms. Many studies have reported on the strong coupling between magnons and various physical quantum systems (such as magnons, photons, phonons, etc.) [10–14].

Strong magnon-magnon coupling can be achieved in several different types of systems [15–19]. Shiota *et al*. realized the regulation of the magnon-magnon coupling between acoustic and optical modes in FeCoB/Ru/FeCoB layers by changing the direction of the in-plane magnetic field and increasing the wave number of excited spin waves [20]. Chen and Klingler *et al*. studied the coupling between spin wave modes of YIG and the ferromagnetic resonance (FMR) of FM materials [21,22]. Furthermore, Adhikari *et al*. reported a mode splitting of dynamic dipolar coupling induced magnon-magnon coupling and spin wave in $Ni_{20}Fe_{80}$ cross-shaped nanoring array [23]. The coupling between FMR and other modes have been extensively studied [20–30]. In general, they addressed the coupling between FMR and higher-order modes, and found the relationship between mode number and coupling strength [22,31]. From here, we explore the possibility of the strong magnon-magnon coupling between FMRs that may be achieved, accordingly; the FMR mode has a wider range of regulatory parameters, such as anisotropy and saturation magnetization. Therefore, it is of interest to study the magnon-magnon coupling between FMRs that leads a promising path toward the strong coupling regime in the pure magnonic system.

In this work, in order to distinguish the FMR modes of two different FM layers, the thicknesses of both the FM layers are designed much thicker than the corresponding exchange length. Meanwhile, we adjusted the anisotropy constant and saturation magnetization to enable the crossing of dispersion relation between FMRs in $Co_{90}Zr_{10}/Ta/Fe_{20}Ni_{80}$ multilayers [Fig. 1(a)]. By using broadband ferromagnetic resonance [32–34], magnon-magnon coupling between FMRs could be realized through the interlayer exchange interaction [35–38] between two FM layers, as shown in Fig. 1(b). The coupling strength, coupling field, and coupling efficiency can be adjusted by changing the sample parameters.

II. METHODS

A. Sample preparation and static magnetic characterization

In order to have crossing between two FMRs in the dispersion relation, CoZr and FeNi are chosen as two different FM layers because the saturation magnetizations of them are quite different and the anisotropic constant of the CoZr can be well regulated. A nonmagnetic (NM) Ta layer is added between the FM layers to tune coupling strength [39]. The $Co_{90}Zr_{10}$(100 nm)/(t_{Ta})/$Fe_{20}Ni_{80}$(100 nm) trilayers with t_{Ta} varied in the range from 0 to 1.6 nm are deposited in a chamber with a base pressure better than 3.8×10^{-7} Torr.

*Correspondence email address: chaigzh@lzu.edu.cn

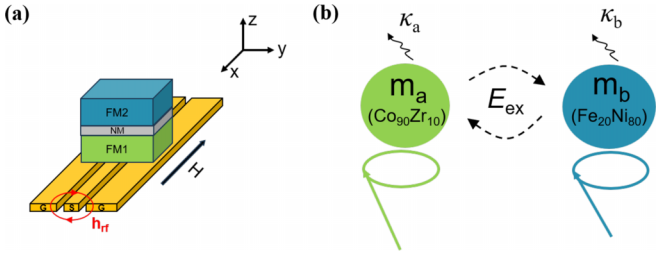

FIG. 1. (a) Sketch of the experimental setup. The microwave generator provides microwave signals to coplanar wave guides (CPW) through microwave cables, and the sample is placed on the CPW. h_{rf} represents the microwave magnetic field, the black arrow represents the direction of the external magnetic field. (b) The schematic of coupling between two different FMRs (m_a and m_b) through interlayer exchange interaction (E_{ex}). κ_a and κ_b represents dissipation of m_a and m_b, respectively.

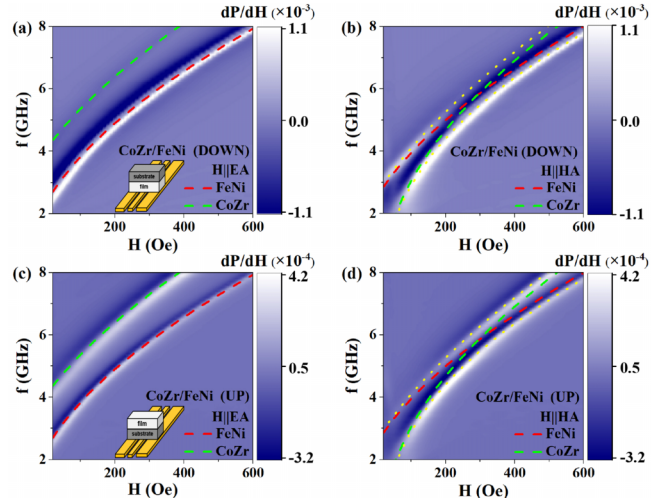

FIG. 2. The results of microwave transmission signals of $Co_{90}Zr_{10}/Fe_{20}Ni_{80}$ bilayer film was measured by FMR measurement. (a), (b) The mapping images measured along the EA (HA) direction and the film surface placed downwards (see inset) with respect to CPW. (c), (d) The mapping images measured along the EA (HA) direction, and the film surface placed upwards (see inset).

The CoZr layer, the Ta layer, and the FeNi layer are deposited using radio frequency magnetron sputtering at a rate of 0.053, 0.022, and 0.148 nm/s, respectively. The working pressure of the sputtering is 1.875 mTorr. All the samples are deposited on naturally oxidized single-crystal Si (111) substrates at room temperature.

By varying the oblique sputtering angle, we regulate the static magnetic properties of monolayer films of CoZr and FeNi. For the CoZr films, we also made adjustments regarding the amount of doped Zr, which is mainly aimed at decreasing the magnetocrystalline anisotropy of Co and refining the grains to enable a better characterization of uniaxial anisotropy [40]. At the same time, the magnitude of saturation magnetization of the CoZr films can be adjusted as well. Finally, the atomic ratio of Co to Zr is 90:10 obtained by energy dispersive x-ray spectrometer (EDX) of scanning electron microscope (SEM, Apero S). And the damping factors of the monolayer $Co_{90}Zr_{10}$ and $Fe_{20}Ni_{80}$, obtained by fitting the permeability spectrum, are 0.019 and 0.011, respectively.

The hysteresis loops of FeNi and CoZr (see Supplemental Material [41]) are characterized by using vibrating sample magnetometer (VSM) to obtain static magnetic parameters such as anisotropic constant, saturation magnetization, coercivity, remanence, etc. When the oblique sputtering angle is increased from 30 degrees to 50 degrees, the anisotropy constant also increases, which is the key factor affecting coupling phenomenon.

B. High frequency magnetic characterization

Permeability is measured by using the vector network analyzer (Agilent E8363B) [42]. By extracting the peak position of the permeability, it is found that the uniaxial anisotropy achieved in the 30 degrees oblique sputtering of CoZr and FeNi satisfied the two f(H) curves crossing in the hard axis (HA) case, which is the basic condition for realizing the coupling between FMRs in the two layer FM film system. In contrast, when the external magnetic field is along the easy axis (EA) of samples, the dispersion relation of the two FMRs do not cross (see Supplemental Material [41]).

III. RESULTS AND DISCUSSION

Transmission signals of $Co_{90}Zr_{10}/Fe_{20}Ni_{80}$ bilayer film were obtained by a highly sensitive broadband ferromagnetic resonance measurement system with lock-in detection [43]. Mapping images are reported in Figs. 2(a) and 2(c) and Figs. 2(b) and 2(d) for the case when the external field is applied along the EA and the HA, respectively. In the fitting of FMR modes (red and green dashed line), we use the Kittel equation as given below [44]:

$$f_K = \gamma[H\cos(\varphi-\varphi_0)+H_{\rm rot}+H_k\cos 2\varphi]^{1/2} \times [H\cos(\varphi-\varphi_0)+H_{\rm rot}+H_\perp+H_k\cos 2\varphi]^{1/2} \quad (1)$$

with parameters listed in Table I to calculate. φ is the angle between the external field applied in the film plane and EA, φ_0 is the angle between EA and magnetic moment confirmed by stoner wohlfarth mode [45]. The gyromagnetic ratio of γ is 2.8 MHz/Oe, H_k is the anisotropic field, $H_{\rm rot}$ is the rotatable anisotropy originated from the interlayer exchange coupling interaction [46,47], and $H_\perp$ is the effective field vertical to the film plane, including magnetic interface anisotropy, perpendicular anisotropy, and demagnetization. Due to the error of anisotropic axis and external magnetic field, it is not a strict direction of the HA, thereby the angle φ is around 90 degrees. Remarkably, the anticrossing phenomenon between two FMRs was observed when the external magnetic field is around 294 Oe and along the HA of the sample, as shown in

TABLE I. Fitted parameters used in Eq. (1).

Material	$H_{\rm rot}$ (Oe)	H_k (Oe)	$H_\perp$ (kOe)	Reference
FMR of $Fe_{20}Ni_{80}$	65	5	11.5	[48]
FMR of $Co_{90}Zr_{10}$	55	85	16	[49]

Fig. 2(b). However, no crossover between two FMRs is observed when the external field is along the EA of the sample, as shown in Fig. 2(a).

We further use the two-state model with Hamiltonian as

$$\mathcal{H} = \begin{pmatrix} f_{K1} & g/2 \\ g/2 & f_{K2} \end{pmatrix}, \tag{2}$$

which give two magnon-magnon coupling eigenmodes:[50]

$$f_{\pm} = \tfrac{1}{2}(f_{K1} + f_{K2}) \pm \tfrac{1}{2}\sqrt{(f_{K1} - f_{K2})^2 + (2g/2\pi)^2}, \tag{3}$$

where f_{K1} and f_{K2} are given by Eq. (1). f_+ and f_- are represented by upper and lower yellow dotted lines (magnon-magnon coupling eigenmodes), respectively [see Figs. 2(b) and 2(d)], and the line width of two white branches (experimental data) indicates the bandwidth of the FMR mode. The coupling strength $g/2\pi$ achieved 0.4 GHz. Moreover, the coupling strength is much greater than the linewidth $g/2\pi > \Delta f$ (the linewidth is 0.19 GHz and 0.16 GHz, respectively), which is achieved strong coupling [51]. And the coupling efficiency $\eta = g/(2\pi f_r)$ reaches 6.9% [52,53].

For the $Co_{90}Zr_{10}$(100 nm)/$Fe_{20}Ni_{80}$ (100 nm) bilayer, it is worth noting that the thickness of each FM layer reaches the order of hundreds of nanometers in order to far exceed their corresponding exchange length so that the FMR between each layer can be measured completely independently which would otherwise fuse into one signal so that magnon-magnon coupling could not be observed [54]. In Figs. 2(a)–2(d), we use "UP" and "DOWN" to show the orientation of one side of the film relative to CPW. The reason is that the signal disappearance caused by the orientation of the sample surface relative to CPW cannot be ignored [see Figs. 2(a) and 2(c)]. When the Si substrate of samples is close to the CPW [see inset of Fig. 2(c)], because the substrate does not conduct electricity, the FMR signal of the CoZr layer, and the FeNi layer can be clearly seen, but the signal strength has weakened relative to the film facing CPW (from the signal values on the color bar, it can be shown). However, when the FeNi layer of samples is close to the CPW [see inset of Fig. 2(a)], the FMR signal of the CoZr layer disappears due to the electric shielding effect of microwave, but this vanishing signal, when the external magnetic field is along the HA of samples, the magnon-magnon coupling leads to a part of the CoZr signal being seen, as shown in Fig. 2(d).

We next study the effect of inserting a Ta interlayer with varying thickness on the magnon-magnon coupling strength in the FM/NM/FM multilayer system. Mapping images of FMR measurement for Ta thickness of $t = 0.4$, 1, and 1.6 nm with external magnetic field applied along HA are shown in Figs. 3(a)–3(c), respectively. All show coupling behavior; we summarize the experimental results by plotting the coupling strength $g/2\pi$ in relation to the inverse of the thickness of the Ta interlayer, as shown in Fig. 3(d). The coupling strength between two FMRs is inversely proportional to the thickness of the Ta interlayer, which is consistent with the law of interlayer exchange interaction [55–58]. By considering phenomenological expression for the interlayer exchange energy, which

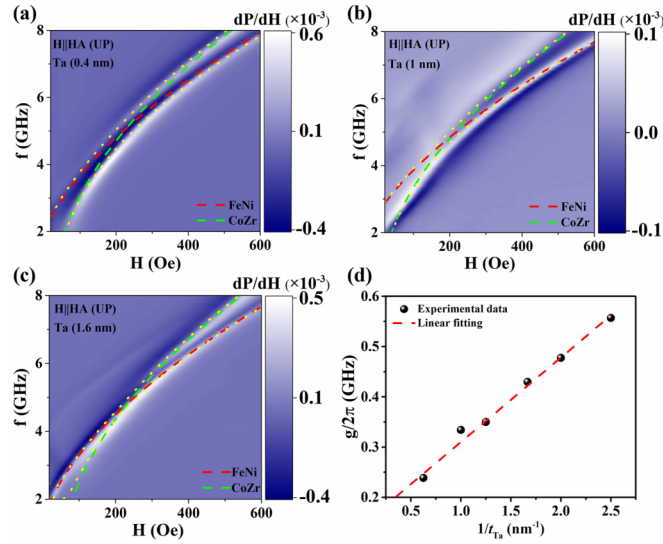

FIG. 3. The mapping images of microwave transmission signals of $Co_{90}Zr_{10}$/Ta/$Fe_{20}Ni_{80}$ measured by FMR measurement. [(a)–(c)] The mapping images of Ta layer thicknesses of 0.4, 1, and 1.6 nm, respectively. (d) The relationship between the coupling strength and reciprocal of the Ta layer thickness.

is given by

$$E_{\text{ex}} = -J_1 \frac{M_1 \cdot M_2}{M_1 M_1} - J_2 \left(\frac{M_1 \cdot M_2}{M_1 M_1}\right)^2, \tag{4}$$

where M_1 and M_2 represent the magnetization vectors of the two ferromagnetic layers, respectively; and J_1 and J_2 represent bilinear and biquadratic coupling coefficient, respectively. If J_1 dominates from the minima of Eq. (4), the coupling is ferromagnetic (antiferromagnetic) for positive (negative) J_1, respectively. If J_2 dominates and is negative, 90 degree type interlayer coupling is obtained. For ferromagnetic material with $J_1 > 0$, in our systems, M_1 and M_2 are parallel to each other not perpendicular, so $J_1 \gg J_2$, the second term of Eq. (4), can be neglected.

In the $Co_{90}Zr_{10}$/Ta(0.6)/$Fe_{20}Ni_{80}$ with oblique sputtering angles 30, 40, 50, and 60 degrees, respectively, we observed the strong magnon-magnon coupling between FMRs when the external magnetic field is along the HA [see Figs. 4(a)–4(d)]. Furthermore, we observed strong coupling between the FMR of CoZr and the first perpendicular standing spin waves mode (first PSSW) of FeNi when the external magnetic field is along the EA. Anticrossing phenomena between the FMR of CoZr (green line) and the first PSSW of FeNi (orange line) are shown in Figs. 4(e)–4(h), and Eq. (3) is used to fit the coupling (yellow dotted line).

In the $Co_{90}Zr_{10}$/Ta/$Fe_{20}Ni_{80}$ multilayer film, the frequency of the nth PSSW f_{P}^n is

$$f_{\text{P}}^n = \gamma[H + H_k + H_{\text{rot}} + H_{\text{ex,n}}]^{1/2} \times [H + H_k + H_{\text{rot}} + H_{\text{ex,n}} + H_{\perp}]^{1/2}, \tag{5}$$

where $H_{\text{ex},n} = \frac{2A}{M_S}(\frac{n\pi}{t_M})^2$ is the saturation magnetization, t_M is the thickness of FM layer, and A is the exchange constant.

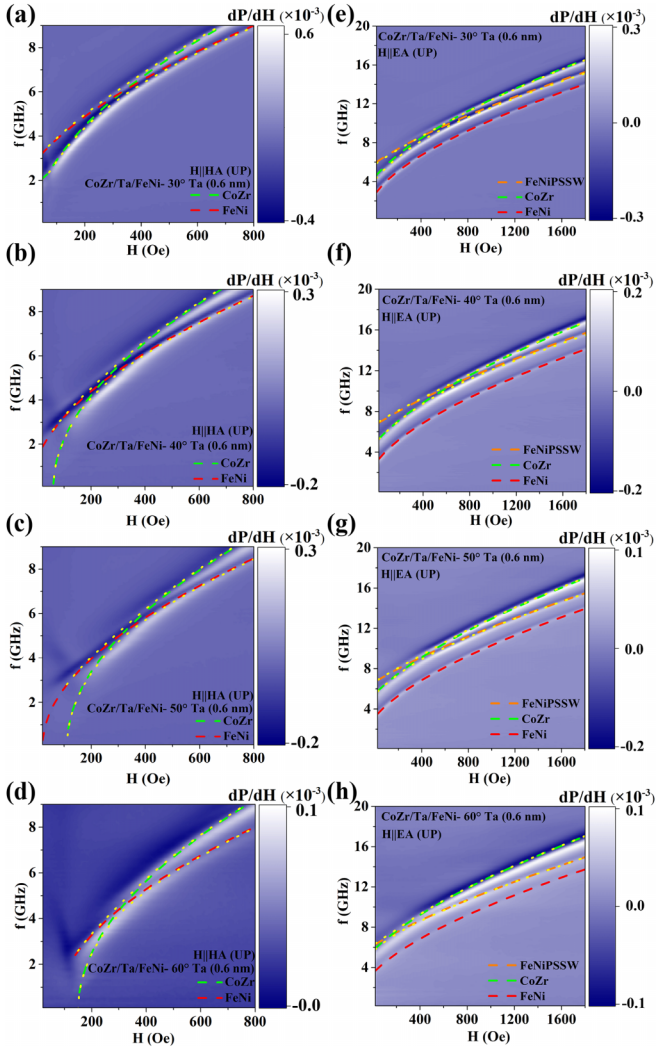

FIG. 4. The mapping images of $Co_{90}Zr_{10}/Ta(0.6)/Fe_{20}Ni_{80}$ with oblique sputtering angles 30, 40, 50, and 60 degrees, respectively. [(a)–(d)] The mapping images measured when the external magnetic field is along the HA of samples. [(e)–(h)] The mapping images measured when the external magnetic field is along the EA of samples.

The fitting parameters of the $Co_{90}Zr_{10}/Ta$ (0.6)/$Fe_{20}Ni_{80}$ with oblique sputtering angle 40 is listed in Table II.

Figure 4 clearly revealed that different oblique sputtering angles of samples lead to different anisotropy fields, which leads to different coupling region. Figure 5 depicts the relation of coupling field and coupling efficiency as a function of oblique sputtering angle θ, which is related to the anisotropy

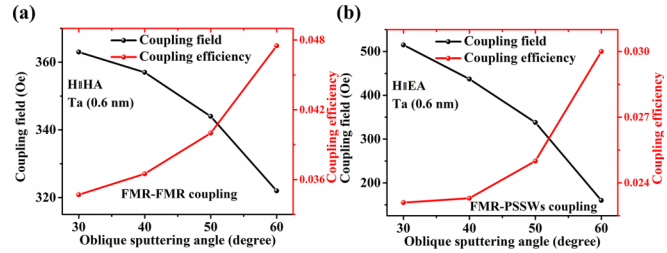

FIG. 5. The relationship between oblique sputtering angles and coupling field and coupling efficiency. (a), (b) The case of the external magnetic field along the HA (EA) axis of samples.

of the sample. Experiment results [Fig. 5(a) for magnetic field applied along EA while Fig. 5(b) for HA] show that η increased with θ as the film fabricated with larger θ result in lower f_r, while $g/2\pi$ does not change significantly for increasing θ. And one can see that the coupling field gradually decreases when the anisotropic field becomes larger. Therefore, without external magnetic field, it is possible to realize the coupling near the zero field between FMR and FMR [see Fig. 5(a)] or PSSWs [see Fig. 5(b)] possibly when the large enough anisotropy field acts as the bias field.

IV. SUMMARY

In summary, we obtained two types of magnon-magnon coupling by changing the external magnetic field configuration. Through the thickness of the FM layer on the order of hundreds of nanometers, the spin number N is large enough and far beyond its exchange length to obtain the strong magnon-mamgnon coupling between FMRs. Based on the interlayer exchange, we realized the control of the coupling strength by changing the thickness of the NM interlayer. Based on changing the magnetic field configuration, we realized the coupling between FMR and PSSWs. We demonstrated the regulation of the coupling parameters by changing the oblique sputtering angle of samples, which make it possible to realize the coupling between FMR and FMR or PSSWs near zero field. Our work also paves the way to build a relationship between two ground-state magnon modes, which could exert a positive influence on the development of magnonics devices.

ACKNOWLEDGMENTS

This work is supported by the National Natural Science Foundation of China (NSFC) (Grant No. 12174165) and the Natural Science Foundation of GanSu Province for Distinguished Young Scholars (Grant No. 20JR10RA649).

TABLE II. Fitted parameters used in the trilayer films.

$Co_{90}Zr_{10}/Ta/Fe_{20}Ni_{80}$	H_k (Oe)	H_{rot} (Oe)	$H_\perp$ (kOe)	M_S (kG)	A (erg/cm)	t_M (nm)	Equation number	Reference
FMR of $Co_{90}Zr_{10}$	125	55	16				(1)	[49]
1st PSSW of $Fe_{20}Ni_{80}$	47.5	52.5	11.5	10	1.6×10^{-5}	90	(5)	[48]

[1] A. V. Chumak, V. Vasyuchka, A. Serga, and B. Hillebrands, Magnon spintronics, Nat. Phys. **11**, 453 (2015).

[2] A. A. Serga, A. V. Chumak, and B. Hillebrands, YIG magnonics, J. Phys. D **43**, 264002 (2010).

[3] V. V. Kruglyak, S. O. Demokritov, and D. Grundler, Magnonics, J. Phys. D **43**, 264001 (2010).

[4] R. P. Feynman, Quantum Mechanical Computers, *Between Quantum and Cosmos*, edited by A. Van Der Merwe, W. H. Zurek, and W. A. Miller (Princeton University Press, 1988) pp. 523–548.

[5] T. D. Ladd, F. Jelezko, R. Laflamme, Y. Nakamura, C. Monroe, and J. L. O'Brien, Quantum computers, Nature (London) **464**, 45 (2010).

[6] H. J. Kimble, The quantum internet, Nature (London) **453**, 1023 (2008).

[7] A. Reiserer and G. Rempe, Cavity-based quantum networks with single atoms and optical photons, Rev. Mod. Phys. **87**, 1379 (2015).

[8] C. L. Degen, F. Reinhard, and P. Cappellaro, Quantum sensing, Rev. Mod. Phys. **89**, 035002 (2017).

[9] S. P. Wolski, D. Lachance-Quirion, Y. Tabuchi, S. Kono, A. Noguchi, K. Usami, and Y. Nakamura, Dissipation-Based Quantum Sensing of Magnons with a Superconducting Qubit, Phys. Rev. Lett. **125**, 117701 (2020).

[10] C. Zhang, Y. Shi, W. Zhang, C. Jiang, and G. Chai, Ultrastrong magnon-photon coupling induced in the photonic crystals with an YGaGeIG defect, Appl. Phys. Lett. **115**, 022407 (2019).

[11] C. Zhang, C. Jia, Y. Shi, C. Jiang, D. Xue, C. K. Ong, and G. Chai, Nonreciprocal multimode and indirect couplings in cavity magnonics, Phys. Rev. B **103**, 184427 (2021).

[12] Y. Shi, C. Zhang, C. Jiang, C. K. Ong, and G. Chai, Mirror symmetric nonreciprocity and circular transmission in cavity magnonics, Appl. Phys. Lett. **119**, 132403 (2021).

[13] H. Man, Z. Shi, G. Xu, Y. Xu, X. Chen, S. Sullivan, J. Zhou, K. Xia, J. Shi, and P. Dai, Direct observation of magnon-phonon coupling in yttrium iron garnet, Phys. Rev. B **96**, 100406(R) (2017).

[14] P. Dai, H. Y. Hwang, J. Zhang, J. A. Fernandez-Baca, S.-W. Cheong, C. Kloc, Y. Tomioka, and Y. Tokura, Magnon damping by magnon-phonon coupling in manganese perovskites, Phys. Rev. B **61**, 9553 (2000).

[15] C. Dai and F. Ma, Strong magnon–magnon coupling in synthetic antiferromagnets, Appl. Phys. Lett. **118**, 112405 (2021).

[16] X. Chen, C. Zheng, S. Zhou, Y. Liu, and Z. Zhang, Manipulation of time- and frequency-domain dynamics by magnon-magnon coupling in synthetic antiferromagnets, Magnetochemistry **8**, 7 (2021).

[17] J. Sklenar and W. Zhang, Self-Hybridization and Tunable Magnon-Magnon Coupling in van der Waals Synthetic Magnets, Phys. Rev. Appl. **15**, 044008 (2021).

[18] M. Li, J. Lu, and W. He, Symmetry breaking induced magnon-magnon coupling in synthetic antiferromagnets, Phys. Rev. B **103**, 064429 (2021).

[19] T. Makihara, K. Hayashida, G. T. Noe II, X. Li, N. Marquez Peraca, X. Ma, Z. Jin, W. Ren, G. Ma, I. Katayama, J. Takeda, H. Nojiri, D. Turchinovich, S. Cao, M. Bamba, and J. Kono, Ultrastrong magnon–magnon coupling dominated by antiresonant interactions, Nat. Commun. **12**, 3115 (2021).

[20] Y. Shiota, T. Taniguchi, M. Ishibashi, T. Moriyama, and T. Ono, Tunable Magnon-Magnon Coupling Mediated by Dynamic Dipolar Interaction in Synthetic Antiferromagnets, Phys. Rev. Lett. **125**, 017203 (2020).

[21] S. Klingler, V. Amin, S. Geprägs, K. Ganzhorn, H. Maier-Flaig, M. Althammer, H. Huebl, R. Gross, R. D. McMichael, M. D. Stiles, S. T. B. Goennenwein, and M. Weiler, Spin-Torque Excitation of Perpendicular Standing Spin Waves in Coupled YIG / Co Heterostructures, Phys. Rev. Lett. **120**, 127201 (2018).

[22] J. Chen, C. Liu, T. Liu, Y. Xiao, K. Xia, G. E. W. Bauer, M. Wu, and H. Yu, Strong Interlayer Magnon-Magnon Coupling in Magnetic Metal-Insulator Hybrid Nanostructures, Phys. Rev. Lett. **120**, 217202 (2018).

[23] K. Adhikari, S. Choudhury, S. Barman, Y. Otani, and A. Barman, Observation of magnon–magnon coupling with high cooperativity in $Ni_{80}Fe_{20}$ cross-shaped nanoring array, Nanotechnology **32**, 395706 (2021).

[24] W. He, Z. K. Xie, R. Sun, M. Yang, Y. Li, X.-T. Zhao, W. Liu, Z. D. Zhang, J.-W. Cai, Z.-H. Cheng, and J. Lu, Anisotropic magnon–magnon coupling in synthetic antiferromagnets, Chin. Phys. Lett. **38**, 057502 (2021).

[25] X. M. Liu, H. T. Nguyen, J. Ding, M. G. Cottam, and A. O. Adeyeye, Interlayer coupling in $Ni_{20}Fe_{80}$/Ru/$Ni_{20}Fe_{80}$ multilayer films: Ferromagnetic resonance experiments and theory, Phys. Rev. B **90**, 064428 (2014).

[26] Y. Li, W. Cao, V. P. Amin, Z. Zhang, J. Gibbons, J. Sklenar, J. Pearson, P. M. Haney, M. D. Stiles, W. E. Bailey, V. Novosad, A. Hoffmann, and W. Zhang, Coherent Spin Pumping in a Strongly Coupled Magnon-Magnon Hybrid System, Phys. Rev. Lett. **124**, 117202 (2020).

[27] H. Y. Yuan, S. Zheng, Z. Ficek, Q. Y. He, and M.-H. Yung, Enhancement of magnon-magnon entanglement inside a cavity, Phys. Rev. B **101**, 014419 (2020).

[28] L. Liensberger, A. Kamra, H. Maier-Flaig, S. Geprägs, A. Erb, S. T. B. Goennenwein, R. Gross, W. Belzig, H. Huebl, and M. Weiler, Exchange-Enhanced Ultrastrong Magnon-Magnon Coupling in a Compensated Ferrimagnet, Phys. Rev. Lett. **123**, 117204 (2019).

[29] D. MacNeill, J. T. Hou, D. R. Klein, P. Zhang, P. Jarillo-Herrero, and L. Liu, Gigahertz Frequency Antiferromagnetic Resonance and Strong Magnon-Magnon Coupling in the Layered Crystal $CrCl_3$, Phys. Rev. Lett. **123**, 047204 (2019).

[30] K. Adhikari, S. Sahoo, A. K. Mondal, Y. Otani, and A. Barman, Large nonlinear ferromagnetic resonance shift and strong magnon-magnon coupling in $Ni_{20}Fe_{80}$ nanocross array, Phys. Rev. B **101**, 054406 (2020).

[31] Y. Cao, P. Yan, H. Huebl, S. T. B. Goennenwein, and G. E. W. Bauer, Exchange magnon-polaritons in microwave cavities, Phys. Rev. B **91**, 094423 (2015).

[32] E. Montoya, T. McKinnon, A. Zamani, E. Girt, and B. Heinrich, Broadband ferromagnetic resonance system and methods for ultrathin magnetic films, J. Magn. Magn. Mater. **356**, 12 (2014).

[33] S. Klingler, A. V. Chumak, T. Mewes, B. Khodadadi, C. Mewes, C. Dubs, O. Surzhenko, B. Hillebrands, and A. Conca, Measurements of the exchange stiffness of YIG films using broadband ferromagnetic resonance techniques, J. Phys. D **48**, 015001 (2015).

[34] V. P. Denysenkov and A. M. Grishin, Broadband ferromagnetic resonance spectrometer, Rev. Sci. Instrum. **74**, 3400 (2003).

[35] M. Belmeguenai, T. Martin, G. Woltersdorf, M. Maier, and G. Bayreuther, Frequency- and time-domain investigation of the dynamic properties of interlayer-exchange-coupled

$Ni_{81}Fe_{19}$/Ru/$Ni_{81}Fe_{19}$ thin films, Phys. Rev. B **76**, 104414 (2007).

[36] M. Vohl, J. Barnaś, and P. Grünberg, Effect of interlayer exchange coupling on spin-wave spectra in magnetic double layers: Theory and experiment, Phys. Rev. B **39**, 12003 (1989).

[37] Z. R. Nunn, C. Abert, D. Suess, and E. Girt, Control of the non-collinear interlayer exchange coupling, Sci. Adv. **6**, eabd8861 (2020).

[38] B. Khodadadi, J. B. Mohammadi, J. M. Jones, A. Srivastava, C. Mewes, T. Mewes, and C. Kaiser, Interlayer Exchange Coupling in Asymmetric Co–Fe / Ru / Co–Fe Trilayers Investigated with Broadband Temperature-Dependent Ferromagnetic Resonance, Phys. Rev. Appl. **8**, 014024 (2017).

[39] T. McKinnon, P. Omelchenko, B. Heinrich, and E. Girt, FMR study of interlayer exchange coupling in FeCoB|Ta|FeCoB trilayers with in-plane anisotropy, J. Appl. Phys. **123**, 223903 (2018).

[40] H. W. Chang, M. H. Wu, C. C. Hsieh, W. C. Chang, and D. S. Xue, High magnetic anisotropy field in CoZr thin films, IEEE Trans. Magn. **47**, 3924 (2011).

[41] See Supplemental Material at http://link.aps.org/supplemental/10.1103/PhysRevB.108.094422 for extra data about static and dynamic magnetic characterizations of samples.

[42] Y. Wang, L. Wang, H. Zhang, Z. Zhong, D. Peng, F. Ye, and F. Bai, Investigation of FeCo–Ti–O nanogranular films with tunable permeability spectrum, J. Alloys Compd. **667**, 229 (2016).

[43] S. Beguhn, Z. Zhou, S. Rand, X. Yang, J. Lou, and N. X. Sun, A new highly sensitive broadband ferromagnetic resonance measurement system with lock-in detection, J. Appl. Phys. **111**, 07A503 (2012).

[44] C. Kittel, On the theory of ferromagnetic resonance absorption, Phys. Rev. **73**, 155 (1948).

[45] E. C. Stoner and E. P. Wohlfarth, A mechanism of magnetic hysteresis in heterogeneous alloys, Philos. Trans. R. Soc. London, Ser. A **240**, 599 (1948).

[46] G. Chai, N. N. Phuoc, and C. K. Ong, Exchange coupling driven omnidirectional rotatable anisotropy in ferrite doped CoFe thin film, Sci. Rep. **2**, 832 (2012).

[47] R. J. Prosen, J. O. Holmen, and B. E. Gran, Rotatable anisotropy in thin permalloy films, J. Appl. Phys. **32**, S91 (1961).

[48] K. Y. Guslienko, V. Novosad, Y. Otani, H. Shima, and K. Fukamichi, Magnetization reversal due to vortex nucleation, displacement, and annihilation in submicron ferromagnetic dot arrays, Phys. Rev. B **65**, 024414 (2001).

[49] R. Ferré, Large scale micromagnetic calculations for finite and infinite 3Dferromagnetic systems using FFT, Comput. Phys. Commun. **105**, 169 (1997).

[50] H. Huebl, C. W. Zollitsch, J. Lotze, F. Hocke, M. Greifenstein, A. Marx, R. Gross, and S. T. B. Goennenwein, High Cooperativity in Coupled Microwave Resonator Ferrimagnetic Insulator Hybrids, Phys. Rev. Lett. **111**, 127003 (2013).

[51] M. S. Skolnick, T. A. Fisher, and D. M. Whittaker, Strong coupling phenomena in quantum microcavity structures, Semicond. Sci. Technol. **13**, 645 (1998).

[52] X. Zhang, C.-L. Zou, L. Jiang, and H. X. Tang, Strongly Coupled Magnons and Cavity Microwave Photons, Phys. Rev. Lett. **113**, 156401 (2014).

[53] T. Niemczyk, F. Deppe, H. Huebl, E. P. Menzel, F. Hocke, M. J. Schwarz, J. J. Garcia-Ripoll, D. Zueco, T. Hümmer, E. Solano, A. Marx, and R. Gross, Circuit quantum electrodynamics in the ultrastrong-coupling regime, Nat. Phys. **6**, 772 (2010).

[54] G. S. Abo, Y.-K. Hong, J. Park, J. Lee, W. Lee, and B.-C. Choi, Definition of magnetic exchange length, IEEE Trans. Magn. **49**, 4937 (2013).

[55] Z. Zhang, P. Wigen, and K. Ounadjela, FMR in strongly coupled Co/Ru/Co structures, IEEE Trans. Magn. **29**, 2717 (1993).

[56] P. Bruno and C. Chappert, Ruderman-Kittel theory of oscillatory interlayer exchange coupling, Phys. Rev. B **46**, 261 (1992).

[57] P. J. H. Bloemen, H. W. van Kesteren, H. J. M. Swagten, and W. J. M. de Jonge, Oscillatory interlayer exchange coupling in Co/Ru multilayers and bilayers, Phys. Rev. B **50**, 13505 (1994).

[58] R. Topkaya, M. Erkovan, A. Öztürk, O. Öztürk, B. Aktaş, and M. Özdemir, Ferromagnetic resonance studies of exchange coupled ultrathin Py/Cr/Py trilayers, J. Appl. Phys. **108**, 023910 (2010).